JOURNAL OF GEOPHYSICAL RESEARCH, VOL. 114, B12301, doi:10.1029/2008JB006192, 2009

Tomography of the westernmost Ryukyu subduction zone and the serpentinization of the fore-arc mantle

Han-Chiang Chou,[1,2] Ban-Yuan Kuo,[3] Ling-Yun Chiao,[4] Dapeng Zhao,[5] and Shu-Huei Hung[1]

Received 3 November 2008; revised 23 July 2009; accepted 5 August 2009; published 1 December 2009.

[1] Three-dimensional tomographic images of the subducting Philippine Sea slab and the fore-arc mantle beneath NE Taiwan and the westernmost Ryukyu were generated in this study. More than 5600 events recorded simultaneously by seismic networks in Taiwan and Japan were relocated for the inversion for variations in V_P, V_S, and V_P/V_S. Analysis of the trade-off between the data variance reduction and model variance helps to determine the appropriate strictness for regularization to avoid either overinterpretatioin or underinterpretation of data. The regularization parameters were also chosen to ensure suppression of artificial V_P/V_S anomalies. The subducting slab is characterized by high V_P, high V_S, and intermediate to low V_P/V_S. Notable in the mantle wedge is the high V_P/V_S anomalies that abut the surface of the subducting slab at depths of 30–80 km. The previously identified positive V_P/V_S channel connecting the slab and the arc volcano interpreted to be a melt pathway is not reproduced in this study. We convert V_S and V_P/V_S to perturbations of temperature and serpentinization of the mantle. The slab is cooled by 200°C–400°C relative to the mantle, in accord with the estimates from theoretical modeling of subduction. The serpentinization reaches ~15%, or 2% water content, at 50 km depth in the fore-arc mantle. We interpret the peak serpentinization as hydrated by the water released from the basalt-eclogite metamorphic reaction in the oceanic crust of the subducting Philippine Sea Plate. The spatial limitation of the present seismic networks in this region with respect to subduction zone events hinders a full description of the pattern of melting in much of the mantle wedge. Resolution tests of the tomographic inversion provide a basis to guide our interpretation to better resolved regions.

Citation: Chou, H.-C., B.-Y. Kuo, L.-Y. Chiao, D. Zhao, and S.-H. Hung (2009), Tomography of the westernmost Ryukyu subduction zone and the serpentinization of the fore-arc mantle, *J. Geophys. Res.*, *114*, B12301, doi:10.1029/2008JB006192.

1. Introduction

[2] The Philippine Sea Plate (PSP) is subducting obliquely beneath the Eurasian Plate along the Ryukyu trench with the western end underlying the island of Taiwan. This framework dictates the tectonics of the region. Not only has the PSP motion brought about the collision between the Luzon arc and the Asian continent [e.g., *Teng*, 1990], but also the subduction has nurtured the initiation of the Okinawa trough (OT) [e.g., *Lee et al.*, 1980; *Sibuet et al.*, 1987]. This nascent back-arc opening, in turn, is propagating westward into the NE corner of Taiwan, or the Yilan plain [*Yeh et al.*, 1989; *Sibuet et al.*, 1998] and interacting with the arc-continent collision in shaping the geology and landscape of northern Taiwan. The collision component of the oblique subduction puts the PSP subducting slab (thereby the Ryukyu slab) under an E-W compression state at lithospheric depths as manifested by earthquake focal mechanisms [*Kao et al.*, 1998]. Using data from both the Taiwan Central Weather Bureau (CWB) network and the Japan Meteorological Agency (JMA) network, *Chou et al.* [2006] relocated thousands of earthquakes and delineate the double seismic zone in the Ryukyu slab from Taiwan 200 km to the east. These authors also quantified the mode of deformation of the slab with folding of a viscoelastic plate under the horizontal compression.

[3] One of the most important elements of a subduction zone-mantle wedge system is the active volcanic front (VF) directly linked to the ongoing subduction process. At the northeastern end of the Ryukyu arc, the present-day VF can be clearly defined by tracing the active volcanoes in southern Kyushu, Japan, southwestward, below which the Wadati-Benioff zone (WBZ) reaches about 100 km depth. The spatial character of these volcanoes is consistent with the mantle-wedge dynamic and petrological paradigm [*Tatsumi and Eggins*, 1995]. However, the definition of the active VF in the westernmost Ryukyu arc is not obvious. The islands of Iriomote and Ishigaki, where JMA stations are located, are presently inactive and are only 60 km above the WBZ [e.g.,

[1]Institute of Geosciences, National Taiwan University, Taipei, Taiwan.
[2]Also at National Cing-Shuei Senior High School, Taichung, Taiwan.
[3]Institute of Earth Sciences, Academia Sinica, Taipei, Taiwan.
[4]Institute of Oceanography, National Taiwan University, Taipei, Taiwan.
[5]Department of Geophysics, Tohoku University, Sendai, Japan.

0148-0227/09/2008JB006192$09.00

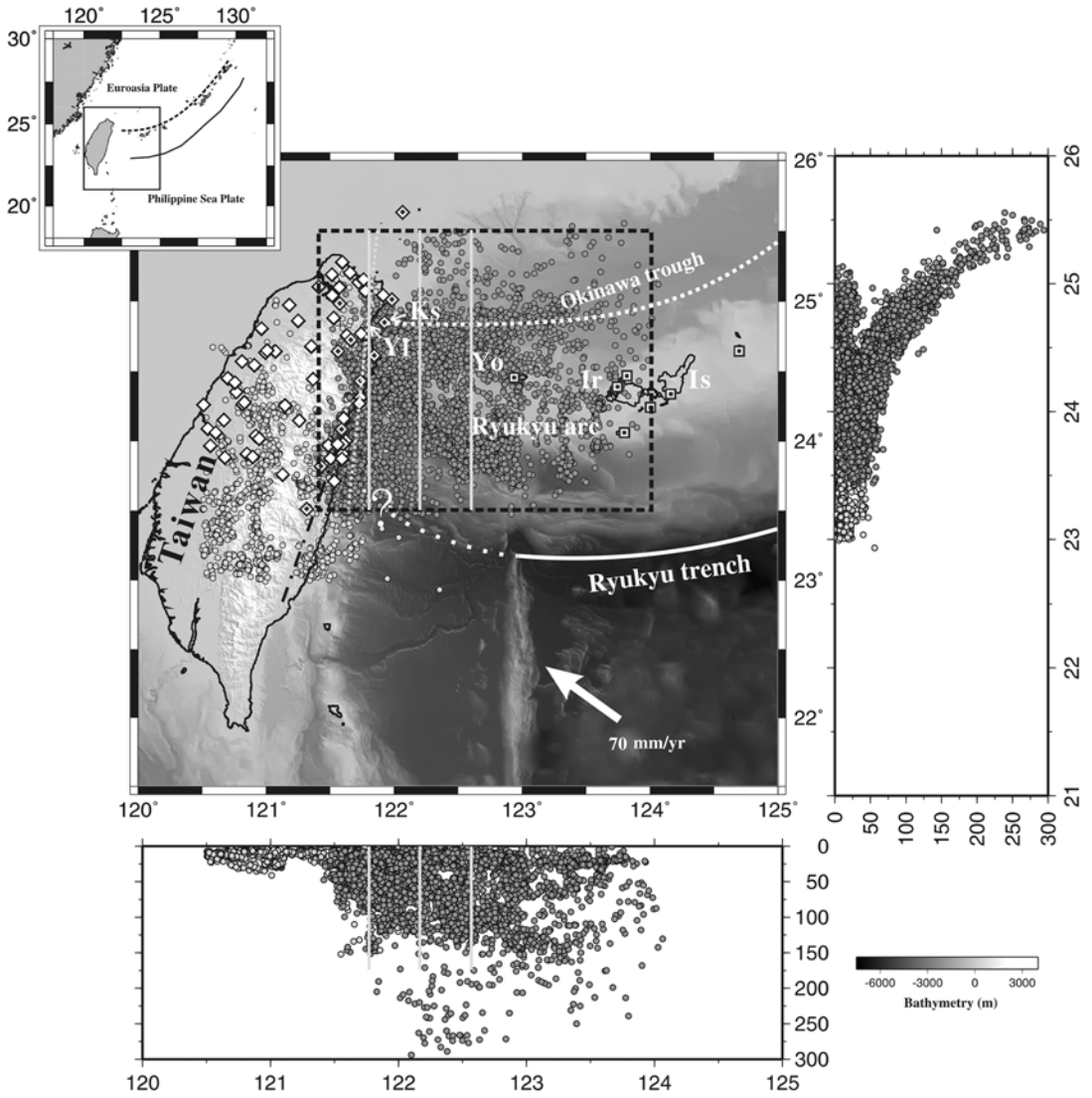

Figure 1. (top left) Index map for the studied region as outlined by the black dashed lines, with local bathymetry, stations, and events. (right) N-S and (bottom) E-W cross sections of seismicity to show subduction zone structures. Seismic stations from the CWB (diamonds) and the JMA (squares) networks form complementary coverage of the region. Filled symbols denote stations used in the joint network inversion. The PSP-Eurasia convergence of 70 mm/yr is shown by the arrow. The western extension of the Ryukyu trench (white line) is ambiguous. The white dotted line in the Okinawa trough indicates the position of the present-day volcanic front [*Chung et al.*, 2000]. Locations of the profiles are denoted as N-S white lines in Figures 1 (top left) and 1 (bottom). Profile 2 of *Lin et al.* [2004] crosses obliquely our 121.8E profile. Ks, Kueishantao; Yl, YiLan Plain; Yo, Yonaguni island; Ir, Iriomote island; Is, Ishigaki island.

Shinjo, 1999]. The present, active VF may lie along a cluster of submerged volcanoes north of these islands, underlain by the Ryukyu slab below ~100 km, with geochemical signatures affiliated with subduction [*Chung et al.*, 2000; *Shinjo*, 1999] (Figure 1). This VF lies mostly south of the axis of the OT, but merges with it when tracked westward to Kueishantao (KST), a 7 ka old andesitic volcano island ~10 km offshore from the coast of the Yilan plain [e.g., *Chung et al.*, 2000; *Chu*, 2005]. The location of the VF is a critical reference in interpreting the tomographic images of the Ryukyu mantle wedge.

[4] This study utilized the CWB-JMA traveltime data with events relocated by *Chou et al.* [2006] to image the slab and the mantle wedge using 3-D seismic tomography. Unlike in Japan where hundreds of land stations are favorably distributed above the subduction zone, most of the westernmost Ryukyu slab lie to the east of the high-density Taiwan network and is covered only by the JMA stations aligned along the Ryukyu arc. This event-station geometry is therefore not overly favorable for imaging the mantle wedge north of the arc. Nonetheless, the joint network approach offers significant advantages regarding offshore areas of Taiwan relative to previous efforts based on CWB alone. The Ryukyu subduction zone beneath northern Taiwan was first imaged with reasonably fidelity by *Rau and Wu* [1995]. Recently, *Lin*

et al. [2004] provided a new model for NE Taiwan using CWB data, while we show in this paper that a joint network approach, despite its uneven aperture toward the east, is helpful to better constrain the structure beneath the margin of the Taiwan network. In a follow-up effort, *Lin et al.* [2007] extended their model to offshore 124°E by incorporating JMA and 12-day OBS data. In addition to the difference in data set, this study differs from *Lin et al.* [2004, 2007] in the inversion strategy and interpretations.

[5] In addition to integration of currently available network data, we emphasize the necessity of achieving the appropriate strictness of the imposed regularization. Despite the impression that the variance reduction versus the model variance trade-off analysis is a routine practice, the discussions concerning the appropriate resolving power of the adopted data sets of regional tomographic studies tend to be downplayed by concealing the actual trade-off pattern. It is thus difficult to clarify whether critical features of a certain tomographic model are in fact effects of either overrepresentation or underrepresentation or interpretation. Examples of possible overinterpretation in previous studies are discussed.

2. Data and Methods

[6] The traveltime data used in this study are the same as that from *Chou et al.* [2006] and are described briefly here. To target the middle zone between Taiwan and Ryukyu, we first selected 11 CWB stations near the NE coast of Taiwan and 7 westernmost stations of JMA as the basis for traveltime data. Events with magnitude 4 or greater within the area from 23.5 to 26.0°N and from 121.5 to 124.0°E registered by at least two stations of each network were selected. This practice avoids overwhelming of the CWB over the JMA data and the potential complications resulting from the highly heterogeneous crust of Taiwan. The final data are selected arrival times reported by both agencies for stations of the joint network. In addition to the data mutually covered by CWB and JMA, a complementary subset of arrival times from the events well within the CWB network in northern Taiwan was also incorporated in the relocation procedure to help illuminate the westernmost edge of the subduction configuration. In all, the data set consists of 7672 relocated events with 74,403 *P* wave and 60,952 *S* wave arrival times.

[7] A preliminary joint inversion for the data set was first executed to determine the hypocentral parameters and the regional one-dimensional (1-D) V_P and V_S structures. The 1-D velocity structure inversion is undertaken by first invoking the projection operator technique that isolates the velocity structure from the hypocentral parameters [*Pavlis and Booker*, 1980]. The vertical velocity profile so obtained is then adopted in the subsequent double difference scheme [*Waldhauser and Ellsworth*, 2000] to relocate all the events. The relocated events better delineate a double-seismic zone, and reveal a fold-like, along-strike deformation of the slab at intermediate depths, possibly rising from impingement with the Eurasian lithosphere [*Chou et al.*, 2006]. The 1-D velocity model is employed as the reference background model for the subsequent 3-D tomography experiments.

[8] The regional traveltime tomography algorithm of *Zhao et al.* [1992] was adopted in this study. Within the area ranging from 23.0 to 26.0°N and from 120.4 to 124.0°E, we constructed a mesh with a horizontal spacing of 0.2° and a vertical spacing of 10 km from the surface to 100 km depth and 20 km from 100 to 200 km depth. We then invert the *P* and *S* traveltimes for V_P and V_S perturbations from the reference 1-D velocity models. Moreover, we sort through the data set and build a subset of travel times from the event-receiver pairs that provide both *P* and *S* arrivals. This subset, consisting of 80% and 98% of the original *P* and *S* sets, respectively, is utilized for the construction of the V_P/V_S model. Notice that

$$\frac{\delta(V_P/V_S)}{(V_P/V_S)} = \frac{V_S\delta V_P - V_P\delta V_S}{V_S^2}\cdot\frac{V_S}{V_P} = \frac{\delta V_P}{V_P} - \frac{\delta V_S}{V_S}. \quad (1)$$

That is, the V_P/V_S anomaly is simply the difference between the V_P and V_S anomalies in fractional form. In other words, robust patterns of $\delta(V_P/V_S)$ perturbations are obtained as long as the constraints invoked to invert for $\delta V_P/V_P$ and $\delta V_S/V_S$ are comparable. This is different from formulations that invert the *P* and *S*-*P* traveltime residuals for the product of $\delta(V_P/V_S)$ and the spatially varying V_P [e.g., *Walck*, 1988], which eventually involves taking ratios of the two inversions. To us, equation (1) can be grasped more intuitively and the algebraic summation of the results from two independent inversions, i.e., $\delta V_P/V_P$ and $\delta V_S/V_S$, is less prone to undesired amplification of the error in each variable than the ratio of two variables. In the Appendix, we devise experiments using the same raypath geometries but with travel times generated from known synthetic structures so that the spatial resolution can be evaluated.

[9] With extensive inversion experiments examining the variance reduction versus the model variance trade-off relation, appropriate damping factors are determined from the trade-off diagram (Figure 2a). The compromise between the model's ability to explain the data and the cost of such ability, i.e., the uncertainty of the model, is reached at the convex portion of the trade-off curves in Figure 2a. Next we test whether the combination of the optimal damping for V_P and V_S is also optimal for V_P/V_S. Figure 2 shows an input model that consists of +8% for a slab and −6% for the overlying mantle in both V_P and V_S. We generate synthetic *P* and *S* travel times for this model for the event-station pairs used in the V_P/V_S inversion, and carry out the inversion as for the real data. According to (1), the same amounts of V_P and V_S fractional anomalies yield a zero V_P/V_S anomaly. Figure 2 shows three combinations of damping all qualified to be "optimal" in the trade-off curves. Among the three examples, the combination in Figure 2d appears to suppress the V_P/V_S anomalies in the mantle more effectively, best matching the zero $\delta(V_P/V_S)$ input model. Less damping in V_P causes more severe a perturbation in V_P, leading to a positive $\delta(V_P/V_S)$, and vice versa, while overdamping of both automatically reduce $\delta(V_P/V_S)$, which is an advantage over the ratio approach. We use the combination in Figure 2d in the inversion and are confident that we will not overinterpret V_P, V_S, and V_P/V_S.

3. Tomographic Models

[10] The tomographic models resulting from the optimal damping indicate that the most predominant features within the area of interest are the high V_P and V_S anomalies associated with the subducting Ryukyu slab down to a depth

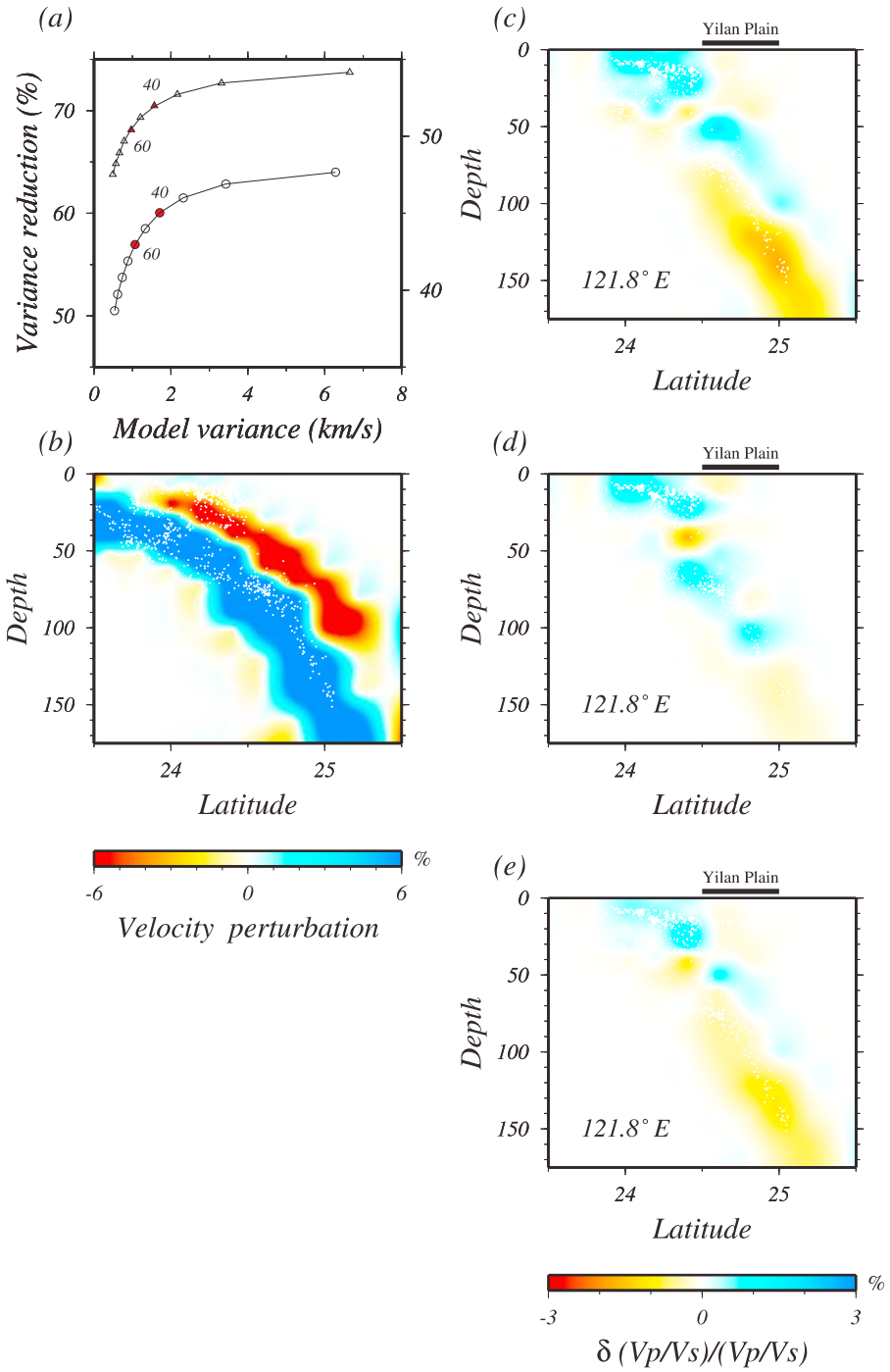

Figure 2. Trade-off tests for V_P, V_S and V_P/V_S. (a) Trade-off curves for V_P and V_S that show compromise between model variance and data variance reduction at the convex portion of the curves. The two values of damping shown are both optimal for individual velocity but may introduce artifact to the ratio of velocities. (b) Input synthetic structure that mimic an exaggerated subduction zone with known zero $\delta(V_P/V_S)$ in both slab and mantle wedge. Inversion outputs are shown with damping (c) 40–40, (d) 40–60, and (e) 60–60 for V_P and V_S, respectively. Artificial nonzero $\delta(V_P/V_S)$ anomalies are created for Figure 2c, and the combinations of the parameters for Figures 2d and 2e suppress the artifacts in both slab and mantle wedge better.

of 150–200 km (Figure 3). We plot the *R*25 line, which delineates the resolving power of 25% as defined in the Appendix, to confine our interpretation in the better resolved regime. Note *R*25 does not guarantee "correct" features, but it is an indicator for what features are worth further examination and what can be disregarded. In this sense only the subduction zone and the neighboring mantle wedge at shallow depths merit interpretation (Figure 3). In addition, the restoration tests in the Appendix show a resolvable scale

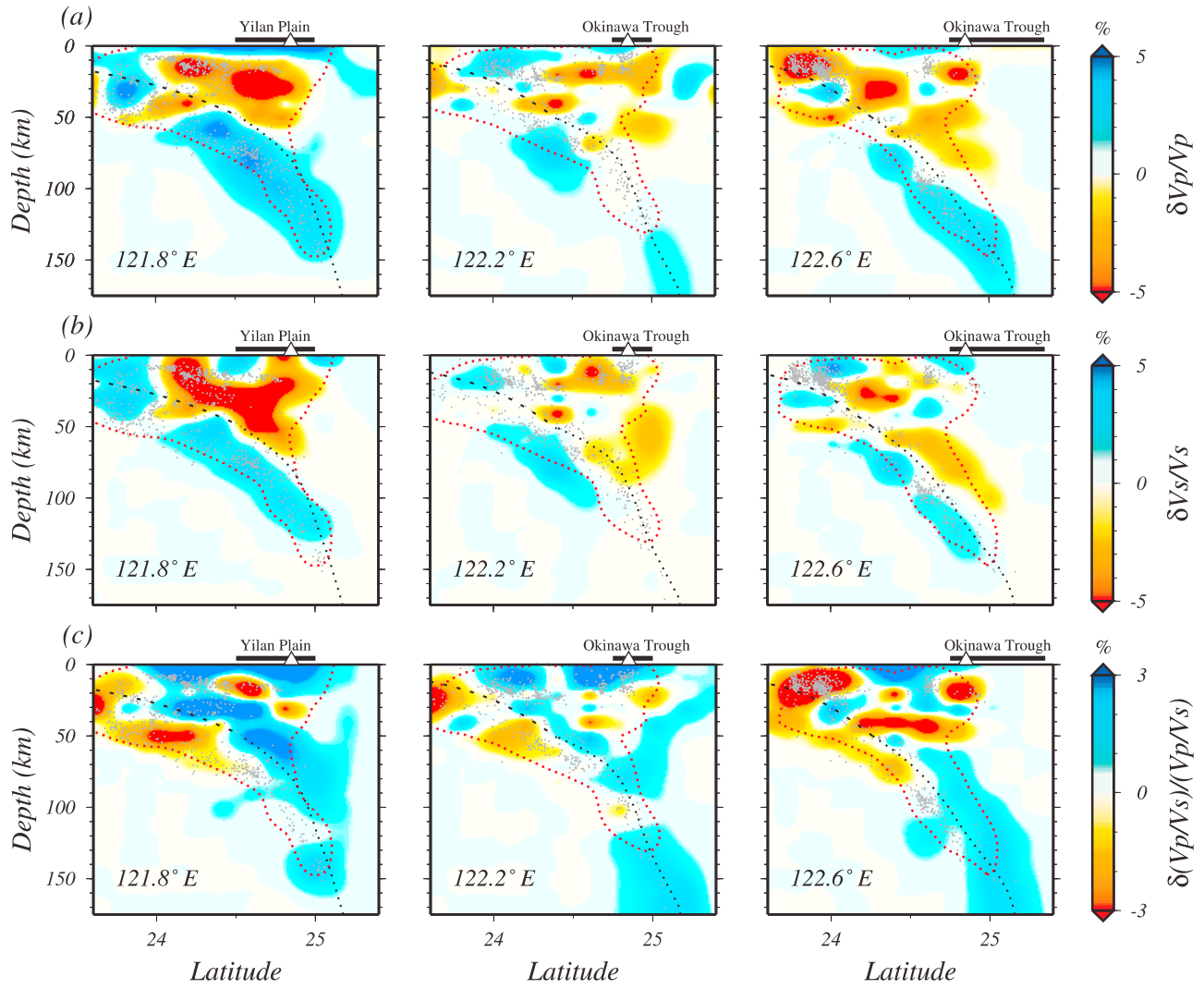

Figure 3. Tomographic images of (a) $\delta V_P/V_P$, (b) $\delta V_S/V_S$, and (c) $\delta(V_P/V_S)/(V_P/V_S)$ shown in three vertical cross sections along longitudes 121.8°E, 122.2°E, and 122.6°E, respectively. *R*25 for V_P is plotted (red dotted line) in each profile to illustrate possible limit of the acceptable recovery of the inversion. The black dotted line is the smoothed slab interface after *Chou et al.* [2006], and the short dashed line is the extrapolation of this interface to the Ryukyu trench at the surface. Locations of relevant tectonic elements are annotated on the top of each diagram. Small triangles represent the VF. Note the slab structure is well resolved only at 121.8°E.

of heterogeneity of 10–20 km in much of the mantle in the *R*25 regime.

[11] The three profiles in Figures 3a and 3b represent typical images of the subduction zone in our model. In the nearshore profile along 121.8°E the slab is resolved to be continuous at 2% perturbation from 50 to 100–150 km depths. Toward the east the slab image is either discontinuous or only continuous at very weak strength (<1%). The disruption of the slab image by neutral or low velocity anomalies below 100 km in the 122.2°E and 122.6°E profiles may result from errors due to uneven distribution of events and stations, and should not be interpreted as a physical break of the slab. Weakened, positive anomalies appear below 150 km, where events exist sparsely (Figure 1). In 121.8°E, there exists a negative anomaly cutting through the shallow segment of the slab at 40–50 km depth beneath 24°N. It is within a broad region of poor 10 km resolution (Figure A1), and the maximum is located near the slab surface in correlation with low seismicity. The strength of this anomaly was solved differently for V_P and V_S, leading to anomalies in V_P/V_S and the parameterized models in the next section. At present we do not have a complete understanding of the origin of this anomaly and we do not interpret it in this study.

[12] In general, the V_P and V_S anomalies in fractional form associated with the subduction zone are similar in amplitude, consistent with a thermal origin because the derivatives with respect to temperature of the two differ only moderately. In the 121.8°E profile, strong negative V_P and V_S anomalies are distributed beneath or close to the Yilan plain (Figures 3a and 3b), and the broad zone of anomaly is avoid of seismicity. As the opening of the OT is thought to propagate westward and has now reached beneath the Yilan plain [*Sibuet et al.*, 1987], the negative anomalies there together with the paucity of seismicity may imply the presence of the relatively hot lower

crust and uppermost mantle in response to the local extensional tectonics. Toward the east where the OT opening is more mature, the correlation of low velocities with the OT is instead not definitive. This is mainly because the OT and the VF progressively move outside the northern limit of the CWB-JMA effective coverage area (Figures 1 and 3).

[13] Because the subducting slab is supposed to be the dominant structure, a reliable model should present a reasonable slab image, and only when the slab is properly imaged do other features on the same profile merit interpretation. We thereafter focus on profile 121.8°E where the slab is resolved to be continuous with realistic velocity anomalies. The most systematic pattern of the positive V_P/V_S perturbation is its juxtaposition with the subducting slab (Figure 3c). It is striking that the dominant features shift from within the slab in V_P and V_S to outside the slab in V_P/V_S. As the synthetic test indicates (Figure 2), the choice of damping for V_P and V_S suppresses amplification of spurious V_P/V_S signature, and therefore the presence of such structure in the model seems warranted. Neutral to negative V_P and V_S with high, positive V_P/V_S anomalies in the mantle wedge have been documented in subduction zones in Japan [*Kamiya and Kobayashi*, 2000], Cascadia [*Zhao et al.*, 2001], and the Andes [*Graeber and Asch*, 1999] through tomographic imaging. *Lin et al.* [2004] also reported low velocities with high V_P/V_S underlying NE Taiwan in their model that bottoms at 60 km depth. High V_P/V_S, together with relatively low V_P and V_S, has been widely interpreted as indicative of hydration of the mantle or in situ melt retention. Water released from the oceanic crust during descending may be absorbed by adjacent mantle peridotite and transform it to serpentinite [*Hacker et al.*, 2003]. This serpentinized layer, if dragged down with the corner flow, will eventually be dehydrated and may trigger water-fluxed partial melting in the wedge [e.g., *Hattori and Guillot*, 2003]. If the wedge is hot enough, water discharged from the subducted crust may facilitate melting in the mantle without an intermediate step of serpentinization [*Arcay et al.*, 2005].

4. Serpentinization

4.1. Parameterization

[14] Our tomographic inversion outputs three types of anomalies, V_P, V_S, and V_P/V_S, with only two of them being independent parameters. V_P/V_S is a more effective indicator of the hydration or melting of a mantle wedge than V_P and V_S alone, and it is independent of either V_P or V_S, but not both. In this section we quantify the effects of hydration of the wedge mantle resulting from dehydration of the subducting crust and slab. Major hydrous minerals in peridotite include serpentine, chlorite, and amphibole. Among these, serpentine dominates the water budget of peridotite [*Schmidt and Poli*, 1998]. In this study, the hydration phenomenon in the fore-arc mantle was parameterized to be the degree of serpentinization of the parent peridotite, Θ. A 100% serpentinite (Θ = 100) has 15 wt% water [e.g., *Hacker et al.*, 2003], and $\Theta = 0$ represents dry peridotite. Water can be provided through subduction by (1) sediment compaction, usually at shallow depths, (2) metamorphic reaction of oceanic crust from blueschist/greenschist to eclogite facies, and (3) dehydration of the previously serpentinized slab mantle at greater depths [*Hyndman and Peacock*, 2003].

[15] We chose V_S and V_P/V_S as the two independent parameters. We take the laboratory measurements of seismic velocities for peridotite serpentinized to various degrees from *Christensen* [1966] and *Horen et al.* [1996]. *Christensen*'s [1966] 2 kbar measurements merge with *Horen et al.*'s [1996] room pressure data well, and the V_P, V_S, and V_P/V_S all display first order linear relationships with Θ. The derivative $d\ln V_S/d\Theta$ of -4.84×10^{-3} is adopted from *Horen et al.* [1996]. The derivative $d\ln(V_P/V_S)/d\Theta$ of 2.254×10^{-3} is determined from a regression of the combined V_P/V_S data provided by *Christensen* [1966] and *Horen et al.* [1996] with a correlation coefficient >0.8. These are one of the two sets of partial derivatives for the degree of serpentinization used in this study and are designated as set I parameters.

[16] *Christensen* [2004] noted that the velocities measured in previous work mainly represent lizardite serpentinite in lower crustal condition rather than antigorite serpentinite stable usually in the fore-arc mantle. Without having the exact data to do regression, we digitized *Christensen*'s [2004] Figure 8 and obtained the following partial derivative values for antigorite serpentinite: $d\ln V_S/d\Theta = -2.59 \times 10^{-3}$ and $d\ln(V_P/V_S)/d\Theta = 0.636 \times 10^{-3}$. Both coefficients were much reduced from their set I counterparts. These partial derivatives are categorized as set II.

[17] Another variable to which velocities are sensitive is temperature. The temperature derivatives are adopted as $d\ln V_S/dT = -1.00 \times 10^{-4}$ °C^{-1} and $d\ln(V_P/V_S)/dT = 2.3 \times 10^{-6}$ °C^{-1} [*Lee*, 2003]. All the coefficients are presumably functions of temperature and pressure, but these functions are not known with higher accuracy and we use their constant forms to transform the tomographic models to tectonically more meaningful variables. Conversion of V_S and V_P/V_S to δT and Θ can be done by solving the equation

$$\begin{bmatrix} \dfrac{\partial \ln V_S}{\partial T} & \dfrac{\partial \ln V_S}{\partial \Theta} \\ \dfrac{\partial \ln(V_P/V_S)}{\partial T} & \dfrac{\partial \ln(V_P/V_S)}{\partial \Theta} \end{bmatrix} \begin{bmatrix} \delta T \\ \delta \Theta \end{bmatrix} = \begin{bmatrix} \delta \ln V_S \\ \delta \ln(V_P/V_S) \end{bmatrix}. \quad (2)$$

The formulation of (2) assumes that temperature and serpentinization are two major independent factors that shape the seismic image of the subduction zone-mantle wedge regime. This is an oversimplification, as other factors, such as compositions and the presence of crack or melt also influence the velocities and ratio. Equation (2) can be considered a rotation of the parameter space such that two new parameters are formed by projection from the original two. Because (2) is an exact system, the matrix inversion will map all the errors in $\delta\ln V_S$ and $\delta\ln(V_P/V_S)$ onto δT and $\delta\Theta$.

[18] Figures 4a and 4b show δT and Θ along 121.8°E generated with the set I Θ parameters. As serpentinization only applies to peridotite and the temperature coefficients are typical of shallow upper mantle conditions, our discussion is restricted to the mantle portion of the model (e.g., >40 km). First, temperature accounts for most of the velocity variations related to the Ryukyu slab, and δT basically follow the pattern of V_S. Along the slab, δT falls into the range of −200°C to −400°C (Figure 4a), which is consistent with what simple subduction zone thermal modeling demonstrates in 100–200 km depth range.

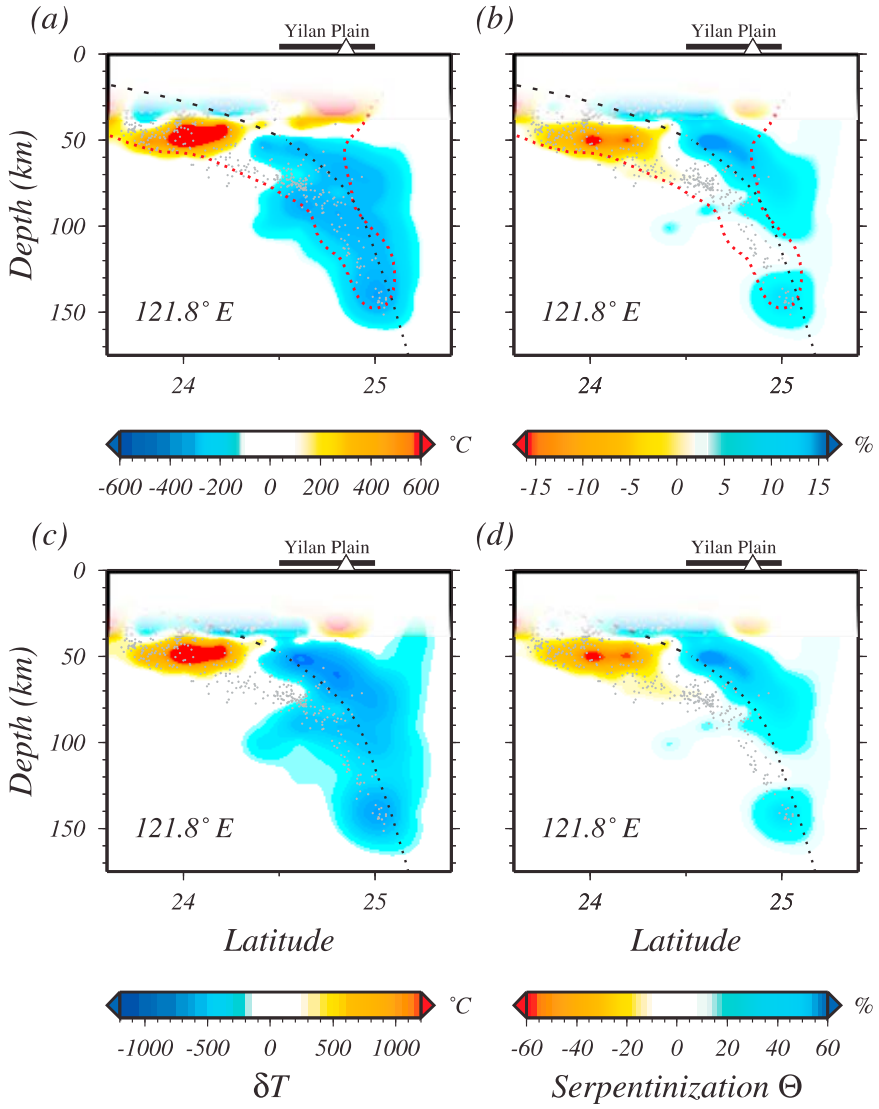

Figure 4. (a) Temperature variation and (b) degree of serpentinization in the mantle determined by equation (2) with set I Θ partial derivatives for 121.8°E. The slab is cooled by 200°C–400°C from the regional mean. The most significant serpentinization zone is in the fore-arc mantle above the slab interface. Models above 40 km depth are not meaningful and are made faded out to the surface. Negative anomalies at the shallow segment of the slab, roughly at 24°N, is unknown in origin. The red thin dotted line is *R*25. (c) Temperature and (d) degree of serpentinization the same as in Figures 4a and 4b, respectively except for set II Θ partials. The temperature minimum on the order of −1000°C in the fore arc is unreasonable.

[19] Serpentinization occurs mainly in the fore-arc mantle adjacent to the slab interface (Figure 4b), and those extending downdip to outside *R*25 are not discussed here. Without the serpentinization parameterization in (2), the fore-arc region with low V_P and V_S would be determined to be warm. Instead, it is now determined to be normal or low temperature. Although only positive Θ makes sense, all signs of Θ were transformed from the right-hand side of (2). An example is the negative Θ at 50 km beneath 24°N (Figure 3). As described above, we are uncertain about the velocity anomalies and therefore reserved about its significance in serpentinization. Strictly, (2) should only be applied to quantify the serpentinization in regions where serpentinization is considered realistic and confidently resolved.

[20] Application of the set II parameters yields different models of temperature and serpentinization (Figures 4c and 4d). Because of the quadruple reduction of the V_P/V_S partial from that in set I, Θ is increased by about fourfold, i.e., to ∼60%, in the fore-arc mantle. The temperature, however, exhibits a strong minimum in the fore-arc mantle where Θ is maximum, instead of within the slab. The extremely cold fore arc may be caused by too high a Θ which entails a V_S too low that requires decreased temperature to compensate for. Judging which set of parameters is correct is beyond the scope of this study, but the set I parameters seem to be preferable in terms of its capability to separate δT and Θ between the slab and the fore-arc mantle in a way consistent with our fundamental knowledge of subduction zones [e.g., *van Keken et al.*,

2002]. These two sets of serpentinization parameters should be tested with other tomographic models.

[21] The serpentinization interpretation for mantle wedge has been invoked elsewhere. In northeast Japan, receiver function images suggest the presence of a long serpentinite layer atop the Pacific slab from 90 to at least 130 km [*Kawakatsu and Watada*, 2007], while in central Japan local, high V_P/V_S are found abutting the surface of the slab at shallow depths [*Kamiya and Kobayashi*, 2000]. Judged from the location of the VF, positive Θ spreads out in the fore arc along the slab interface and reaches a maximum at roughly 50 km depths. This may be linked to the progressive breakdown of hydrous minerals, i.e., lawsonite, chlorite, zoisite, and amphibole in basalt during the basalt-eclogite metamorphic transformation that releases water to hydrate the mantle immediately above it [*van Keken et al.*, 2002; *Iwamori*, 2007]. This is reminiscent of the Cascadia mantle wedge where reflectivity evidence implies strong serpentinization in the fore-arc region at depths 30–50 km [*Bostock et al.*, 2002]. Geological evidence of the fore-arc serpentinization was also found in both oceanic and continental convergent margins [*Fryer et al.*, 1999; *Guillot et al.*, 2000]. In this study, we cannot argue whether serpentinization spreads along the arc because of the decreasing resolution of tomography toward the east.

4.2. Melting

[22] If the temperature is higher than the stability field of the hydrous minerals in serpentinite, serpentinization would not occur in the first place. The free water may facilitate water-fluxed melting at temperatures above water-saturated solidus, or escape upward at lower temperatures. This is an intricate dynamic process, which has been the subject of much numerical modeling effort [e.g., *van Keken et al.*, 2002; *Peacock et al.*, 2005; *Arcay et al.*, 2005]. Beneath NE Japan, low V_P, V_S, and high V_P/V_S anomalies subparallel to the slab in the mantle wedge were interpreted to be a melt signature [e.g., *Zhao et al.*, 2009] with a melt fraction ϕ of 1–2% [*Nakajima et al.*, 2005]. The serpentinized layer later detailed by *Kawakatsu and Watada* [2007] in the same region was localized between the melt zone and the slab. Technically, degree of melting can be estimated by replacing the partial derivatives for Θ with those for ϕ. Examination of the melt model of *Nakajima et al.* [2005] indicates that the signs of the partials of V_S and V_P/V_S with respect to ϕ are consistent with the signs of the partials with respect to Θ, implying that what can be converted to high serpentinization may be converted to a high melt fraction as well.

[23] However, we refrain from addressing the issue of melting based on two observations. First, the melt zone in NE Japan is in the hot core of the wedge beneath the VF and beyond, and is at least 50–100 km horizontally away from the slab interface. In contrast, in NE Taiwan and the westernmost Ryukyu, the well resolved high V_P/V_S signature is adjacent to the slab and at shallower depths localized in the fore arc. Although the mantle wedge here may be warmer near the edge, there are no present-day volcanic activities documented above the fore-arc region. Second, the VF here is small in magnitude compared with the abundant VF activities in NE Japan [*Sibuet et al.*, 1998; *Chung et al.*, 2000; *Tatsumi and Eggins*, 1995; *Tamura et al.*, 2002], implying probably low melt generation at least at present stage. On the other hand, the limited aperture of observation does not allow us to sample northward far into the wedge interior to fully depict the melt distribution. In the present work we attribute the low V_P, V_S, and high V_P/V_S anomaly atop the slab interface to serpentinization of the peridotitic mantle. The pattern and properties of melting in this region may only be defined in the future with a larger-aperture imaging incorporating an OBS array in the OT.

5. Discussion

[24] Unlike in Japan, Alaska, and Cascadia, the JMA part of the combined network provides limited aperture to constrain the mantle wedge north of the subduction zone. Our strategy is to present models that do not overrepresent and inflate what the data can possibly offer. The variance reductions of less than 70% and 60% for V_P and V_S, respectively, are low enough to suppress uncertain, secondary features in the model. We do not interpret anything outside the *R*25 limit, and within the *R*25 limit we are careful in not overinterpreting subtle features whose scale is less than the resolvable scale of heterogeneity. In practice, we are confident more in the profiles in which the subducting Ryukyu slab is resolved better, i.e., showing continuous high V_P and V_S anomalies. Profile 121.8°E is an example, and is the focus of the discussion in this study.

[25] In a recent tomographic effort, *Lin et al.* [2004] obtained a relatively high V_P/V_S channel rising from the slab interface at 40 km depth obliquely to the Yilan plain (with KST 15 km away). The presence of the channel is intriguing by itself, but its signature is weak against the average wedge mantle. With the integrated data sets of CWB and JMA and a carefully calibrated V_P/V_S inversion, we examine whether this feature is robust and worth further elaboration. Note the recoverable scale of heterogeneity is approximately 10 km in this part of the model and the grid spacing is 10 km, which is an adequate parameterization to resolve the melt pathway of *Lin et al.* [2004].

[26] Figure 5 compares the tomographic images of this study and *Lin et al.* [2004] in the same vertical slice shown in the latter. The slab is resolved much better in this study, lending credence to other images. We cannot see any features suggestive of a channel structure connecting the slab and the surface, crossing the corner of the mantle wedge. Throughout all the profiles, no features alike stand out as an obvious anomaly. We also test using different combinations of damping factors for V_P and V_S, i.e., taking models in the neighborhood of the optimums at the two trade-off curves in Figure 2a. One of them is a model with the V_P/V_S norm the same as *Lin et al.* [2004] in the 2-D slice. While the inclined high V_P/V_S layer overlying the slab largely remains, features suggesting a melt pathway claimed by *Lin et al.* [2004] cannot be reproduced. In their study, the primary structure of the Ryukyu slab is poorly resolved in the same profile where the secondary feature of melt is emphasized.

[27] In their most recent work, *Lin et al.* [2007] combined CWB, JMA, and OBS data to constrain the velocity structure in the region similar to that of this study but for the upper 60 km. Their OBS data, recorded over a period of 12 days, may provide additional constraints on the crustal structure of the OT. This advantage, if properly parameterized into the inversion, provides a potential for better imaging the fore arc

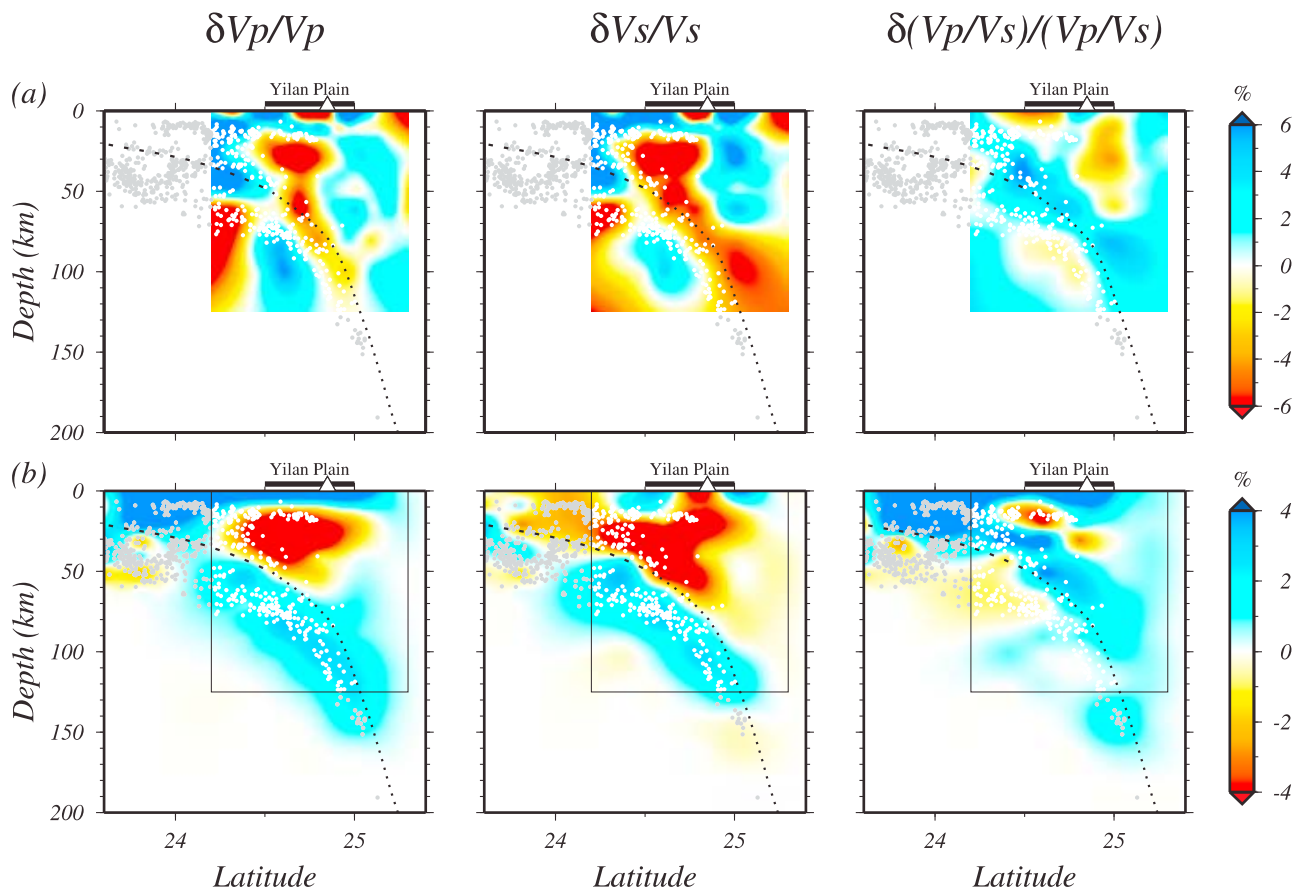

Figure 5. Comparison in V_P, V_S, and V_P/V_S between (a) *Lin et al.* [2004] and (b) this study, along profile 2 of the former. See position of profile in Figure 1. Note the primary feature such as the high V_P/V_S atop the slab is resolved in both studies despite different shapes, while the secondary feature, the weak, positive V_P/V_S anomaly extending obliquely from the slab to the surface in the study by *Lin et al.* [2004] is not resolved in this study. The slab as the most important structure is better expressed in this study than that in the study by *Lin et al.* [2004].

and the slab. *Lin et al.* [2007] reported the presence of more "channels" of melts that feed the VF or the back-arc axis from various parts of the slab along the strike. Yet a comparison between *Lin et al.*'s [2007] study and this study is not straightforward, because their "channels" are highly variable in 3-D and overly subtle, and are very likely beyond the resolution of our model. Here we do not attempt to trace and connect patchy anomalies into a seemingly continuous structure and attach significance to them.

[28] Our model shows that the serpentinization reaches 15% in the fore arc of the westernmost Ryukyu subduction zone. This is comparable to what is estimated from the V_P anomaly alone [*Zhao et al.*, 2001] and less than the local maximum Θ inferred from a reflectivity result [*Bostock et al.*, 2002] both in the Cascadia subduction zone. As serpentinite (Θ = 100) contains 15 wt% water [e.g., *Hacker et al.*, 2003], the maximum water content in the fore-arc mantle may be 2%, and locally the content may be greater because the tomography heavily damps the variations. This amount of bound water may be stable in between the serpentine chlorite dunite field (~6%) and the chlorite harzburgite field (~1.4%) at 50 km depths (~1.5 GPa) and between 500°C and 800°C [*Hacker et al.*, 2003]. As a reference, this temperature range is lower than the water-saturated solidus of peridotite, i.e., 900°C–1000°C at shallow mantle pressures [*Kawamoto and Holloway*, 1997; *Grove et al.*, 2006].

[29] A self-consistent scenario with the serpentinization hypothesis will be that significant water is liberated from basaltic crust at or below 50 km. This will require a temperature range in the oceanic crust which spans the breakdown of hydrous minerals that involve abundant water losses. However, the 500°C–800°C range mostly spans the low water content (<1%) eclogite field at 1.5–2 GPa (~50–65 km) [*Hacker et al.*, 2003]. A reasonable conjecture is that the temperature of the oceanic crust straddles the blueschist/greenschist-eclogite boundary, i.e., 400°C–500°C between 1.5 and 2 GPa [*Hacker et al.*, 2003] so that abundant water (~5%) can be expelled to hydrate the fore-arc mantle. The temperatures may increase from below 400 to above 500°C passing through this depth range. At 50 km or so, water-saturated solidus for basalt is ~650°C [*Lambert and Wyllie*, 1972]. Minor dehydration melting may occur upon zoisite-out reaction at ~700°C–750°C, but it is not until >900°C when amphibole breaks down that the crust melts significantly [*Vielzeuf and Schmidt*, 2001; *Hacker et al.*, 2003]. Although intensive melting seems unlikely, small amount of melting of the oceanic crust cannot be fully rejected.

[30] Geochemical evidence for crust melting in the western Ryukyu subduction zone has not been completely established. High-Mg andesites, considered as an indicator for slab melting, were reported at Iriomote, a previous VF 13 Ma in age now located at the fore arc, but their geochemical signature does not support a subduction zone origin [*Shinjo*, 1999]. However, the recent work on KST (VF) rocks indicated that some of the samples contain high-Mg components, implying some degree of slab melt contribution to the arc volcanoes [*Chu*, 2005]. The issue is still open and developments on this geochemical front should be closely watched. Numerical modeling, geochemical constraints, and seismological imaging need to be integrated to further the understanding of melting in the mantle wedge or slab beneath the westernmost Ryukyu.

[31] Can the fore-arc serpentinization be tested in the future against other observations? Tomography can be improved with OBS deployment in the OT, but the same velocity-based approach likely yields a pattern similar to that in this study. A critical test can be attained from a seismic attenuation tomography. The low attenuation, or high Q value, in the fore-arc mantle beneath Alaska and Cascadia constrained by array waveforms is thought to arise from low temperature, which agrees with the low heat flow measured at the surface [*Schurr et al.*, 2003; *Stachnik et al.*, 2004]. Both Q model and heat flow measurement across the OT are lacking at present and will critically test the serpentinization hypothesis in the future.

6. Conclusion

[32] By integrating CWB and JMA data we construct a tomographic model for the subduction zone and mantle wedge between the NE Taiwan and the westernmost Ryukyu with the best resolution near offshore Taiwan. In light of the relatively unfavorable network coverage, we take a conservative approach toward both regularizing the inversion and interpreting the results. The high V_P and V_S anomalies associated with the subducting Ryukyu slab dominates the tomographic images, while the high V_P/V_S signals above the slab characterize the mantle wedge. The high V_P/V_S channel depicted in a previous tomographic effort and interpreted to be a melt pathway feeding the Yilan plain from the slab cannot be reproduced in this study. The slab signature is consistent with a temperature anomaly of -200°C to -400°C. Significant anomalies of low V_P, V_S and high V_P/V_S appear in the fore arc of the mantle wedge, south of the present-day volcanic front. We interpret this signature as the hydration of mantle peridotites by the water discharged from the basalt-eclogite metamorphism in the subducted oceanic crust, and parameterize it as percentage of serpentinization using laboratory data. Peak serpentinization may reach more than 15%, or 2% water content, in the fore-arc wedge near NE Taiwan. This is a notable departure from previous views which emphasize the role of melts. To achieve a full imaging of the mantle wedge and the melt distribution, expansion of the array with OBSs in the future is critical.

Appendix A

[33] Nonuniform raypath coverage of most regional traveltime tomography studies results in obviously uneven spatial sampling of the velocity perturbations. A conventional approach is to perform restoration experiments on simple synthetic structures such that the spatially varying resolving power of the obtained tomographic model can be appraised.

[34] In addition to the test on V_P/V_S illustrated in Figure 2, we set up a restoration experiment as follow. A synthetic 3D checkerboard model with ±6%, fast and slow alternating velocity anomalies over the grids of our model, i.e., horizontal spacing 0.2° and vertical spacing 10 and 20 km above and below 100 km depth, respectively. As a comparison, a model with a grid spacing doubled is also performed. Traveltime residuals were generated from this model using the raypath sampling identical to the real data. Random errors with zero mean and 0.8 s standard deviation are blended in the synthetic traveltime residuals. Since the geometry of the raypath distribution is the same as in the real inversions, additional trade-off analysis is redundant. That is, we simply adopt the same damping parameters as the ones for the actual inversion (Figure 2a). Errors and damping are essential for conducting a checkerboard test, which are often missed in previous studies. It is clear that our damping parameters efficiently remove potential artifacts from poorly sampled areas at the expense of losing certain marginal resolving power. Figures A1 and A2 show restoration experiments for the two sets of grid spacing. Overall, 10 km resolution diminishes rapidly toward east, while 20 km is maintained better. In the near TW profile, resolvable scale of heterogeneity is 10 km in the crust, 10–20 km in the fore-arc mantle, and probably 20 km in the slab throughout. In the eastern profiles, 20 km variation is in general discernable, except degrading with depth in the slab. The resolution ranges from poor beneath the VF in most of the profiles to none deep in the wedge.

[35] The checkerboard analysis helps to determine the scale of heterogeneity a model can achieve. To quantify how closely to the true value each model parameter is resolved, one needs to establish the resolution matrix, defined as $R = G_g^{-1}G$, where G_g^{-1} is the generalized inverse of the G matrix in the inversion system $Gm = d$. If the system is solved with a singular value decomposition, R can be easily obtained. Usually, nonzeros in R spread over physically neighboring grids, ideally with a maximum value at the center grid. The grid with R value of 1 implies that this parameter is independently resolved and therefore the true model value is recovered, if no errors in data. The diagonal values of the R matrix therefore map out the resolvability at each grid of the tomographic model. In this study the values for the V_P model are used to represent the overall model resolvability. In Figures A1 and A2, most of the region above 50 km in the western end of the model has R values >0.5, where station control is the best. The V_S and V_P/V_S anomalies interpreted to be high serpentinization in the fore arc (Figure 3, 121.8°E profile) straddles the $R \sim 0.5$ contour. The mantle wedge immediately next to the slab and largely above 100 km makes the $R = 0.25$ requirement. We take $R = 0.25$ ($R25$) to be the limit of the resolvable part of the model and the limit of the region within which anomalies are worth an interpretation with caution. Because R is determined by the ray geometry a priori to the inversion, $R25$ should be considered a weak criterion, because structures within this limit could be affected by data errors.

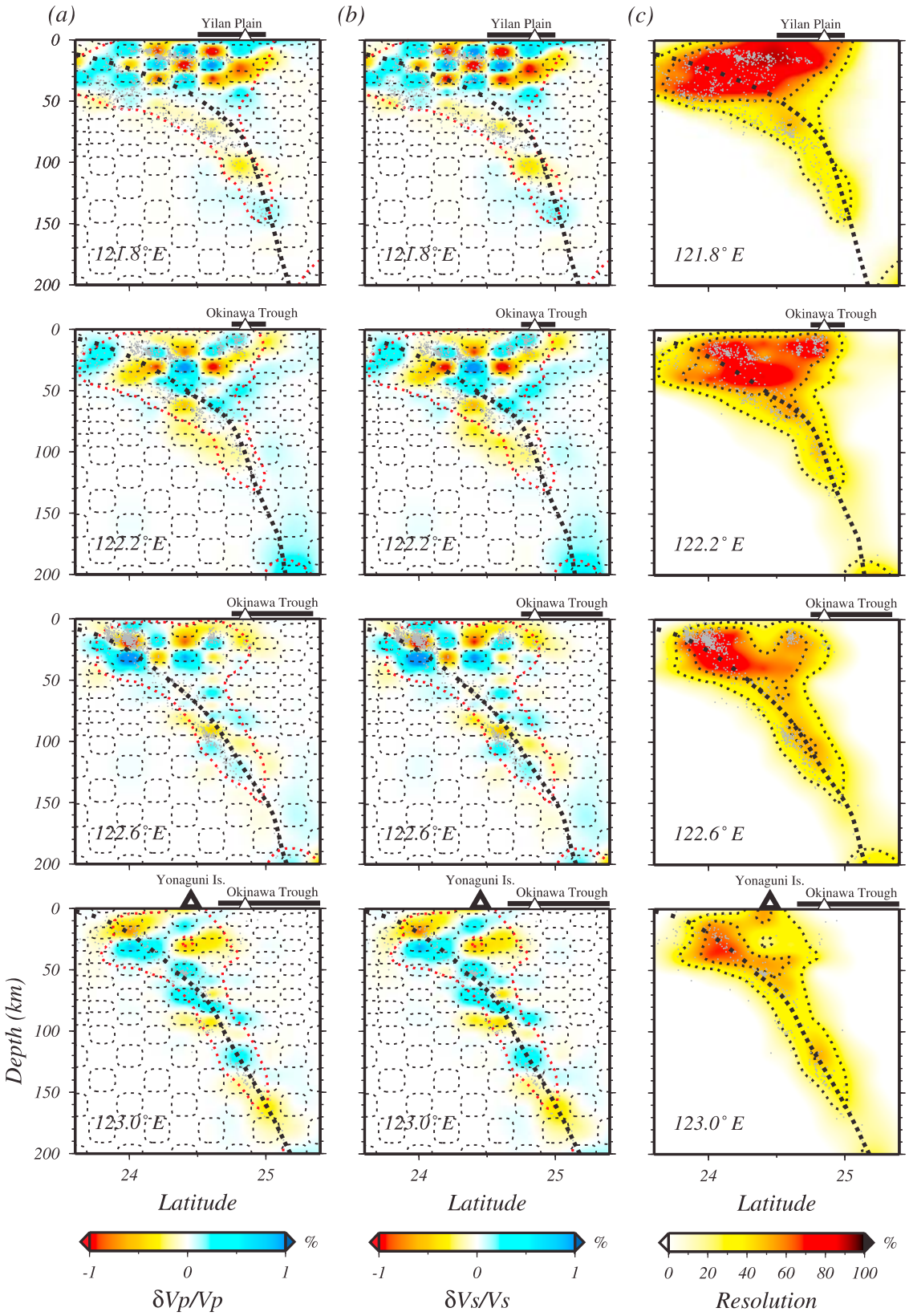

Figure A1. Checkerboard restoration test. (a and b) Velocities and (c) the values of the diagonal terms of the model resolution matrix R for V_P. Above 100 km, grid spacing is 0.2° by 0.2° by 10 km in depth, as outlined by the black dotted lines. Below 100 km, grid spacing is 0.2° by 0.2° by 20 km. The R values are contoured at 25% and 50% (Figure A1c), and the 25% contour is shown in the velocity Figures A1a and A1b ($R25$) as red dotted lines. Note the blurring or shifting of adjacent opposite anomalies in some of the profiles near the margin of the $R25$ region and in profiles to the east.

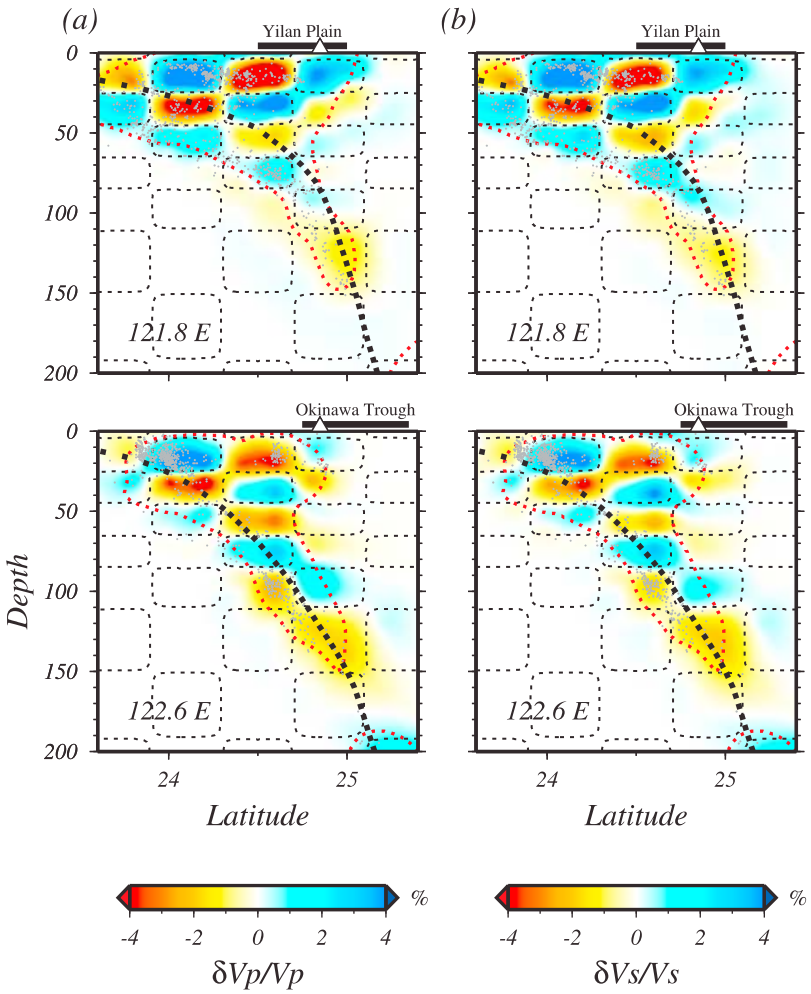

Figure A2. Checkerboard restoration test as in Figure A1 but with grid spacing grids doubled, shown for selected slices (a) for V_P and (b) for V_S. The model has adequate resolving power for this scale of heterogeneity within $R25$ (red dotted lines) in most of the depths and profiles, but the resolution still degrades to the east.

[36] **Acknowledgments.** We are grateful to K. L. Wang, who helped to clarify the geochemical background of this study. Discussions with W. T. Liang, S. L. Chung, and S. R. Song are also appreciated. All graphs were created using the Generic Mapping Tool package [*Wessel and Smith*, 1991]. This study is supported by the National Science Council of Taiwan, under the contract NSC 97-2745-M-001-012.

References

Arcay, D., E. Tric, and M. P. Doin (2005), Numerical simulations of subduction zones: Effects of slab dehydration on the mantle wedge dynamics, *Phys. Earth Planet. Inter.*, *149*, 133–153, doi:10.1016/j.pepi.2004.08.020.

Bostock, M. G., R. D. Hyndman, S. Rondenay, and S. M. Peacock (2002), An inverted continental Moho and serpentinization of the forearc mantle, *Nature*, *417*, 536–538, doi:10.1038/417536a.

Chou, H. C., B. Y. Kuo, S. H. Hung, L. Y. Chiao, D. Zhao, and Y. M. Wu (2006), The Taiwan-Ryukyu subduction-collision complex: Folding of a viscoelastic slab and the double seismic zone, *J. Geophys. Res.*, *111*, B04410, doi:10.1029/2005JB003822.

Christensen, N. I. (1966), Elasticity of ultrabasic rocks, *J. Geophys. Res.*, *71*, 5921–5931.

Christensen, N. I. (2004), Serpentinites, peridotites, and seismology, *Int. Geol. Rev.*, *46*, 795–816, doi:10.2747/0020-6814.46.9.795.

Chu, C. H. (2005), Generation of high-Mg andesites in the Kueishantao volcano, the southernmost part of the Okinawa Trough (in Chinese), Master's thesis, 99 pp., Natl. Taiwan Univ., Taipei.

Chung, S. L., S. L. Wang, R. Shinjo, C. S. Lee, and C. H. Chen (2000), Initiation of arc magmatism in an embryonic continental rifting zone of the southernmost part of Okinawa trough, *Terra Nova*, *12*, 225–230, doi:10.1046/j.1365-3121.2000.00298.x.

Fryer, P., C. G. Wheat, and M. J. Mottl (1999), Mariana blueschist mud volcanism: Implication for conditions within the subduction zone, *Geology*, *27*, 103–106, doi:10.1130/0091-7613(1999)027<0103:MBMVIF>2.3.CO;2.

Graeber, F. M., and G. Asch (1999), Three-dimensional models of P wave velocity and P-to-S velocity ratio in the southern central Andes by simultaneous inversion of local earthquake data, *J. Geophys. Res.*, *104*, 20,237–20,256, doi:10.1029/1999JB900037.

Grove, T. L., N. Ghatterjee, S. W. Parman, and E. Médard (2006), The influence of H_2O on mantle wedge melting, *Earth Planet. Sci. Lett.*, *249*, 74–89, doi:10.1016/j.epsl.2006.06.043.

Guillot, S., K. H. Hattori, and J. de Sigoyer (2000), Mantle wedge serpentinization and exhumation of eclogites: Insights from eastern Ladakh, northwest Himalaya, *Geology*, *28*, 199–202, doi:10.1130/0091-7613(2000)28<199:MWSAEO>2.0.CO;2.

Hacker, B. R., G. A. Abers, and S. M. Peacock (2003), Subduction factory: 1. Theoretical mineralogy, densities, seismic wave speeds, and H_2O contents, *J. Geophys. Res.*, *108*(B1), 2029, doi:10.1029/2001JB001127.

Hattori, K. H., and S. Guillot (2003), Volcanic fronts form as a consequence of serpentinite dehydration in the forearc mantle wedge, *Geology*, *31*, 525–528, doi:10.1130/0091-7613(2003)031<0525:VFFAAC>2.0.CO;2.

Horen, H., M. Zamora, and G. Dubuisson (1996), Seismic wave velocities and anisotropy in serpentinized peridotites form Xigaze ophiolite: Abundance

of serpentine in slow spreading ridge, *Geophys. Res. Lett.*, *23*, 9–12, doi:10.1029/95GL03594.

Hyndman, R. D., and S. M. Peacock (2003), Serpentinization of the forearc mantle, *Earth Planet. Sci. Lett.*, *212*, 417–432, doi:10.1016/S0012-821X(03)00263-2.

Iwamori, H. (2007), Transportation of H_2O beneath the Japan arcs and its implications for global water circulation, *Chem. Geol.*, *239*, 182–198, doi:10.1016/j.chemgeo.2006.08.011.

Kamiya, S., and Y. Kobayashi (2000), Seismological evidence for the existence of serpentinized wedge mantle, *Geophys. Res. Lett.*, *27*, 819–822, doi:10.1029/1999GL011080.

Kao, H., S.-J. Shen, and K.-F. Ma (1998), Transition from oblique subduction to collision: Earthquakes in the southernmost Ryukyu arc-Taiwan region, *J. Geophys. Res.*, *103*, 7211–7229, doi:10.1029/97JB03510.

Kawakatsu, H., and S. Watada (2007), Seismic evidence for deep-water transportation in the mantle, *Science*, *316*, 1468–1471, doi:10.1126/science.1140855.

Kawamoto, T., and J. R. Holloway (1997), Melting temperature and partial melt chemistry of H_2O-saturated mantle peridotite to 11 gigapascal, *Science*, *276*, 240–243, doi:10.1126/science.276.5310.240.

Lambert, I. R., and P. J. Wyllie (1972), Melting of gabbro (quartz eclogite) with excess water to 35 kilobars, with geological applications, *J. Geol.*, *80*, 693–708, doi:10.1086/627795.

Lee, C. S., G. J. Shor, L. D. Bibee, R. S. Lu, and T. W. C. Hilde (1980), Okinawa trough: Origin of a back-arc basin, *Mar. Geol.*, *35*, 219–241, doi:10.1016/0025-3227(80)90032-8.

Lee, C. T. A. (2003), Compositional variation of density and seismic velocities in natural peridotites at STP conditions: Implications for seismic imaging of compositional heterogeneities in the upper mantle, *J. Geophys. Res.*, *108*(B9), 2441, doi:10.1029/2003JB002413.

Lin, J. Y., S. K. Hsu, and J. C. Sibuet (2004), Melting features along the western Ryukyu slab edge (northeast Taiwan): Tomographic evidence, *J. Geophys. Res.*, *109*, B12402, doi:10.1029/2004JB003260.

Lin, J. Y., J. C. Sibuet, C. S. Lee, S. K. Hsu, and F. Klingelhoefer (2007), Origin of the southern Okinawa trough volcanism from detailed seismic tomography, *J. Geophys. Res.*, *112*, B08308, doi:10.1029/2006JB004703.

Nakajima, J., Y. Takei, and A. Hasagawa (2005), Quantitative analysis of the inclined low-velocity zone in the mantle wedge of northeastern Japan: A systematic change of melt-filled pore shapes with depth and its implications for melt migration, *Earth Planet. Sci. Lett.*, *234*, 59–70, doi:10.1016/j.epsl.2005.02.033.

Pavlis, G. L., and J. R. Booker (1980), The mixed discrete-continuous inverse problem; application to the simultaneous determination of earthquake hypocenters and velocity structure, *J. Geophys. Res.*, *85*, 4801–4810, doi:10.1029/JB085iB09p04801.

Peacock, S. M., P. E. van Keken, S. D. Holloway, B. R. Hacker, G. A. Abers, and R. L. Rergason (2005), Thermal structure of the Costa Rica-Nicaragua subduction zone, *Phys. Earth Planet. Inter.*, *149*, 187–200, doi:10.1016/j.pepi.2004.08.030.

Rau, R. J., and F. T. Wu (1995), Tomographic imaging of lithospheric structure under Taiwan, *Earth Planet. Sci. Lett.*, *133*, 517–532, doi:10.1016/0012-821X(95)00076-O.

Schmidt, M. W., and S. Poli (1998), Experimentally based water budgets for dehydrating slabs and consequences for arc magma generation, *Earth Planet. Sci. Lett.*, *163*, 361–379, doi:10.1016/S0012-821X(98)00142-3.

Schurr, B., G. Asch, A. Rietbrock, R. Trumbull, and C. Haberland (2003), Complex patterns of fluid and melt transport in the central Andean subduction zone revealed by attenuation tomography, *Earth Planet. Sci. Lett.*, *215*, 105–119, doi:10.1016/S0012-821X(03)00441-2.

Shinjo, R. (1999), Geochemistry of high Mg andesites and the tectonic evolution of the Okinawa Trough-Ryukyu arc system, *Chem. Geol.*, *157*, 69–88, doi:10.1016/S0009-2541(98)00199-5.

Sibuet, J.-C., et al. (1987), Back-arc extension in the Okinawa trough, *J. Geophys. Res.*, *92*, 14,041–14,063, doi:10.1029/JB092iB13p14041.

Sibuet, J.-C., B. Deffontaines, S. Hsu, N. Thareau, J. Le Formal, C. Liu, and the ACT Party (1998), Okinawa trough backarc basin: Early tectonic and magmatic evolution, *J. Geophys. Res.*, *103*, 30,245–30,267.

Stachnik, J. C., G. A. Abers, and D. H. Christensen (2004), Seismic attenuation and mantle wedge temperatures in the Alaska subduction zone, *J. Geophys. Res.*, *109*, B10304, doi:10.1029/2004JB003018.

Tamura, Y., Y. Tatsumi, D. Zhao, Y. Kido, and H. Shunkuno (2002), Hot fingers in the mantle wedge: New insights into magma genesis in subduction zones, *Earth Planet. Sci. Lett.*, *197*, 105–116, doi:10.1016/S0012-821X(02)00465-X.

Tatsumi, Y., and S. Eggins (1995), Subduction Zone Magmatism, 211 pp., Blackwell, Cambridge, U. K.

Teng, L. (1990), Geotectonic evolution of late Cenozoic arc-continent collision in Taiwan, *Tectonophysics*, *183*, 57–76, doi:10.1016/0040-1951(90)90188-E.

van Keken, P. E., B. Kiefer, and S. M. Peacock (2002), High-resolution models of subduction zones: Implications for mineral dehydration reactions and the transport of water into the deep mantle, *Geochem. Geophys. Geosyst.*, *3*(10), 1056, doi:10.1029/2001GC000256.

Vielzeuf, D., and M. W. Schmidt (2001), Melting relations in hydrous systems revisited: Application to metapelites, metagreywackes and metabasalts, *Contrib. Mineral. Petrol.*, *141*, 251–267.

Walck, M. (1988), Three-dimensional V_P/V_S variations for the Coso region, California, *J. Geophys. Res.*, *93*, 2047–2052, doi:10.1029/JB093iB03p02047.

Waldhauser, F., and W. L. Ellsworth (2000), A double-difference earthquake location algorithm: Method and application to the northern Hayward fault, *Bull. Seismol. Soc. Am.*, *90*, 1353–1368, doi:10.1785/0120000006.

Wessel, J. K., and H. F. Smith (1991), Free software helps map and display data, *Eos Trans. AGU*, *72*, 445–446, 441, doi:10.1029/90EO00319.

Yeh, Y. H., C. H. Lin, and S. W. Roecker (1989), A study of upper crustal structures beneath northeastern Taiwan: Possible evidence of the western extension of Okinawa trough, *Proc. Geol. Soc. China*, *32*, 139–156.

Zhao, D., A. Hasegawa, and S. Horiuchi (1992), Tomographic imaging of P and S wave velocity structure beneath northeastern Japan, *J. Geophys. Res.*, *97*, 19,909–19,928, doi:10.1029/92JB00603.

Zhao, D., K. Wang, G. C. Rogers, and S. M. Peacock (2001), Tomographic image of low P velocity anomalies above slab in northern Cascadia subduction zone, *Earth Planets Space*, *53*, 285–293.

Zhao, D., Z. Wang, N. Umino, and A. Hasegawa (2009), Mapping the mantle wedge and interplate thrust zone of the northeast Japan arc, *Tectonophysics*, *467*, 89–106, doi:10.1016/j.tecto.2008.12.017.

L.-Y. Chiao, Institute of Oceanography, National Taiwan University, P.O. Box 23-13, Taipei 10617, Taiwan.

H.-C. Chou and S.-H. Hung, Institute of Geosciences, National Taiwan University, No. 1, Sec. 4, Roosevelt Rd., Taipei 10617, Taiwan.

B.-Y. Kuo, Institute of Earth Sciences, Academia Sinica, 128 Academia Rd., Sec. 2, Taipei 11529, Taiwan. (byk@earth.sinica.edu.tw)

D. Zhao, Department of Geophysics, Tohoku University, 6-6 Aoba, Aramaki, Aoba-ku, Sendai 980-8578, Japan.